

Optical Engineering

OpticalEngineering.SPIEDigitalLibrary.org

Clocking-optimization method for figure-error balancing in complex optical systems

Xiaolin Liu
Yanqiu Li
Ke Liu

Clocking-optimization method for figure-error balancing in complex optical systems

Xiaolin Liu, Yanqiu Li,* and Ke Liu

Beijing Institute of Technology, School of Optoelectronics, Teaching Building No. 7, Room 206, 5 South Zhongguancun Street, Haidian District, Beijing 100081, China

Abstract. Figure errors of optical surfaces degrade the performance of optical systems. When predicting the performance and performing system assembly, compensation by clocking of optical components around the optical axis is a conventional but user-dependent method. Commercial optical software cannot optimize this clocking, and existing automatic figure-error balancing methods have limitations. To overcome these limitations, a global and general optimization method based on analyzing the precise relationships between the figure errors and the wavefront error (WFE) is proposed. Using the footprint data of each optical surface, the resulting WFE is calculated. Direct map operation is used for intercepting and rotating the figure-error maps. The simulated annealing algorithm is used to seek the optimal combination of clocking angles for the optical components. This method can be applied to most coaxial optics systems, including dioptric, catoptrics, and catadioptric complex lenses. It is successfully implemented for a catadioptric immersion lithographic optics system with artificial figure errors, and for an experimental lithographic optics system with actual manufacturing figure errors. © The Authors. Published by SPIE under a Creative Commons Attribution 3.0 Unported License. Distribution or reproduction of this work in whole or in part requires full attribution of the original publication, including its DOI. [DOI: [10.1117/1.OE.54.5.057103](https://doi.org/10.1117/1.OE.54.5.057103)]

Keywords: optical fabrication; figure error; aberration compensation; lithography.

Paper 150320 received Mar. 12, 2015; accepted for publication Apr. 13, 2015; published online May 7, 2015.

1 Introduction

Figure errors form the low-frequency component of optical-surface errors and degrade the performance of an optical system.^{1,2} Their impact is highly significant in complex optics applications that involve many surfaces, as in catadioptric lithographic optics systems, which can combine up to 50 optical surfaces. Within optical manufacturing and mechanical-clamping processes, compensation methods are necessary and crucial for reducing the effect of figure errors. Three compensation methods have been developed: repolishing surfaces,³ laser-induced contraction of the coating,⁴ and clocking of optical components.^{5,6} Exploiting the idea that the figure errors of multiple optical surfaces can be compensated in a mutual manner, optical-component clocking around the optical axis has become a conventional method in the stages of performance prediction and system assembly. However, currently available commercial optical software cannot optimize clocking for mutual figure-error compensation. In practice, the traditional way to implement component clocking is by rotating various combinations of the components manually, a process that relies strongly on the experience of the user. Manual operation is clearly random, blind, and not very efficient, especially for complex optical systems. There is therefore a pressing need to determine the optimal combination of clocking angles for optical components before they are assembled. Recently, a clocking-optimization method for dioptric optics was developed.⁷ However, it only considered the relationship between the wavefront error (WFE) and the figure error of a refractive surface, expressed as an empirical formula for a wavelength of 193 nm. Therefore, that method cannot be used for dioptric optics lenses at other wavelengths, catoptrics lenses, or

catadioptric lenses. We previously derived a universal theory for analyzing the dependence of the WFE on the figure error of optical components.⁸ This included refractive surfaces, internal reflective surfaces, and external reflective surfaces. The theory can be used to analyze the WFE caused by figure errors during clocking optimization. Meanwhile, we previously developed a clocking-optimization method.⁸ In the previous optimization method, the clocking procedure indirectly optimizes the clocking angle of an individual WFE map induced by figure error and performed a 360-deg tour to determine the best position. However, the previous optimization method is only applied in optical systems with a small field of view. For optical systems with a large field of view, the light radiation area (footprint) of each field point is different. Moreover, it is not full of the entire clear aperture. When the optical component is rotated, the figure-error map on the footprint area is changed. Meanwhile, the individual WFE map caused by the optical component with figure error is changed. Therefore, the individual WFE map cannot be indirectly rotated to replace the optical-component clocking, for the large-field system. Moreover, in the previous method, the optical component that least affects the WFE is performed at a 360-deg tour individually, rather than simultaneous rotation of all optical components. Therefore, the final result may be not the global optimal solution.

In this paper, we present a general method of clocking optimization that compensates for figure errors automatically. This method can be used in almost all coaxial optical imaging systems, including dioptric, catoptrics, and catadioptric complex lenses without vignetting and with a large field of view. In this method, the analytical relationships between the figure error and the WFE established serve as the fundamentals of computation theory. Based on this relationship and footprint data obtained from optical-design software, we can calculate the WFE that results from the figure

*Address all correspondence to: Yanqiu Li, E-mail: liyanqiu@bit.edu.cn

errors. Direct map operation is then used to intercept and rotate the figure-error maps. The globally optimal combination of clocking angles can then be obtained by using the simulated annealing algorithm. This method is described in detail in Sec. 3. Section 4 demonstrates the feasibility and effectiveness of this method using simulations of two catadioptric lithographic projection optics (PO) systems.

2 Relationship Between Figure Error and Wavefront Error

The optical surface with figure error can be treated as a thin asymmetrical phase plate attached on the nominal surface. The figure error can induce an additional WFE, also known as optical path difference. To develop a clocking optimization procedure beyond the scope of commercially available software, the relationship between figure errors and the WFE must first be established. For a lens, these linear relationships were deduced and verified in detail in a previous study.⁸ For a given field of view, the relationship between the figure error of one surface and the WFE is described for a refractive surface as

$$W_{S_R} \approx (1 - n) \cdot S_F. \quad (1)$$

For an internal reflective surface, such as a Mangin mirror,⁹ the relationship is given by

$$W_{S_{\text{inR}}} \approx -2n \cdot S_F, \quad (2)$$

and for an external reflective surface, such as a traditional mirror, the relationship is given by

$$W_{S_{\text{exR}}} \approx 2S_F, \quad (3)$$

where S_F is the figure error in the illuminated region (termed “footprint” in optical-design software), n is the refractive index of the optical material, and W_S is the WFE resulting from the figure error of one surface. By using Eqs. (1)–(3), the change in WFE can be obtained without new ray trajectories.

Considering actual physical operation, only optical components can be rotated in the process of figure-error balancing. An optical component may include two or more surfaces, such as a cemented doublet. Optical-component clocking can be treated as the synchronized rotation of all included surfaces with figure error. The total surface number of one optical component is indicated by m . The net WFE caused by figure error of the optical component is the sum of the individual W_S :

$$W_E = \sum_{i=1}^m W_{S_i}. \quad (4)$$

Furthermore, for the physical surface through which the light would pass more than one time, it should be taken as multiple surfaces rather than one surface in Eq. (4). For example, if a surface is passed through twice, it must be taken as two surfaces in clocking optimization, and the m in Eq. (4) is modified as $m + 1$.

Finally, for a given field point, the WFE of the overall optical system produced by all the figure errors is given by

$$W_{\text{system}} = \sum_{j=1}^N W_{E_j}, \quad (5)$$

where N is the total number of optical components in the optical system, and W_{E_j} is the contribution to the WFE of the figure error of the j 'th optical component.

The accuracy of this method is sufficient for calculating the WFE induced by figure errors at any working wavelength.⁸

3 Clocking-Optimization Method

After all the optical components have been manufactured, predicting performance before system assembly is crucial for high-precision and expensive optical systems. This task can indicate the best position and clocking angle for each component in the initial lens assembly. The position of each component can be optimized according to the measuring thickness and curvature radius. Based on measuring figure errors, the optimal clocking angle of each component can then be calculated using our clocking-optimization method, described in a subsequent paragraph.

Figure errors are generally asymmetrically distributed. Therefore, the figure errors of all the optical surfaces can be balanced and compensated in a mutual manner. Using the linear relationships given in Sec. 2, the effect on the WFE can be calculated. Surface figures and refractive indices are measured before this clocking optimization.

A surface figure is generally measured using a Fizeau interferometer. The measurement accuracy of the figure error can reach subnanometer levels. Refractive index measurement accuracy can reach 10^{-6} . Therefore, the measurement errors can be ignored in the clocking-optimization process. As a specific example, the mechanical stress generated by the lens-mounting seats may induce additional error on the optical surface. Therefore, to achieve better compensation, it is advisable to measure the surface figures of optical components coupled in the lens seat and to include them in the optimization of figure-error balancing. For high-precision optical systems, such as a lithographic projection lens, lens-mounting seats¹⁰ are designed to be stress-free such that stress-related index changes and surface deformations can be neglected. It is generally advisable to measure surface figures in their proper setting within the optical system, so that disturbances due to stress and temperature are appropriately considered in figure-error balancing. In this manner, the measurements of surface figures and refractive indices reflect the actual features of the optical system more correctly, to enable a much more effective compensation.

A figure error is generally expressed using a set of 36 Zernike polynomials, and the normalized diameter is the measured clear aperture. It should be noted that the initial measured orientation must be labeled, on the edge of an optical component or lens seat, as the initial azimuth of that component rotation.

In the clocking-optimization method, the acquisition of the figure error on the footprint area under a certain clocking angle is the most critical step during the rotation process. Every field point corresponds to a footprint of each optical surface. The footprint area can be determined using commercially available optical-design software.

Here, we take lithographic PO as an example to describe the acquisition of the figure error on the footprint area. Based

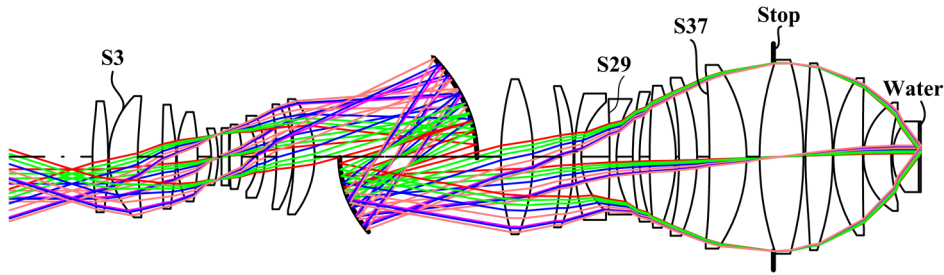


Fig. 1 Layout of NA 1.2 lithographic projection optics.

on the research in Ref. 11, we designed a NA 1.2 immersion PO with an image field of size 26×5.5 mm for a wavelength of 193.368 nm. This PO includes 23 refractive optical components and two concave mirrors. The WFEs in the whole field range are less than 0.005λ ($\lambda = 193.368$ nm) without vignetting at the design stage. The layout of the PO is shown in Fig. 1. The off-axis rectangular field in the image plane is shown in Fig. 2. Fifteen field points were sampled to represent the overall system performance. Here, three representative surfaces located in different position of this optical system are chosen to illustrate the acquisition of the figure error on the footprint area. The footprints on these three surfaces are shown in Fig. 3. Surface 3 in Fig. 3(a) is near the field plane, Surface 29 in Fig. 3(b) is located

between the field plane and the stop plane, and Surface 37 in Fig. 3(c) is near the stop plane. For optical systems without vignetting, the footprints are approximately circles. Therefore, the position and size of a footprint can be described by the center coordinates and radius of the corresponding circle. Generally, the position and size of the footprint of each field point vary as the rays pass through the successive optical surfaces, and do not change with surface or component clocking. When an optical component is rotated around the optical axis, the distribution of the figure error in the footprint scope is changed. To intercept the figure error in a footprint area from the entire clear aperture labeled in Fig. 3(a), a “mask” for each footprint is required. Using the boundary coordinates of the footprint, the center coordinates and the radius of the intercepting area can be calculated. The boundary of the intercepting mask can then be determined by the parameters. Although the footprint size is different on each surface, an equal number of sampling point must be used in the effective intercepted area on each mask, for the purpose of the calculation of W_5 using Eqs. (4) and (5). Therefore, the sizes of the mask matrices of the footprints are different. Moreover, a larger mask matrix is needed to sample adequately for a smaller footprint area. For a given field point, 128×128 sampling points are set in the intercepting area on the mask of each surface. The mask matrix of a footprint on a surface is expressed as $A \times A$. A is the size of the mask matrix, which can be calculated by

$$A = CA \cdot \frac{128}{2R_f}, \quad (6)$$

where CA is the diameter of the clear aperture of this surface, R_f is the radius of a footprint on this surface, and the units of CA and R_f are mm. Figure 4 shows the masks on the three

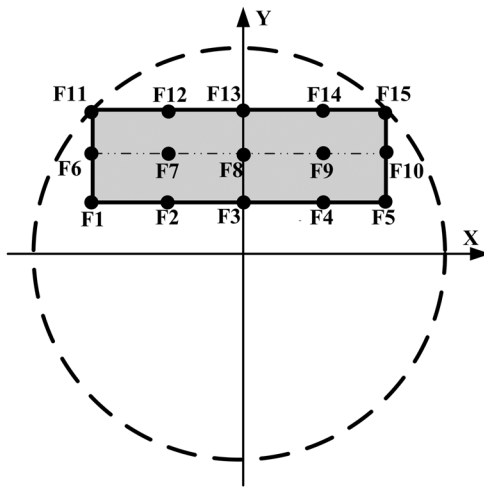


Fig. 2 Field points on the image plane.

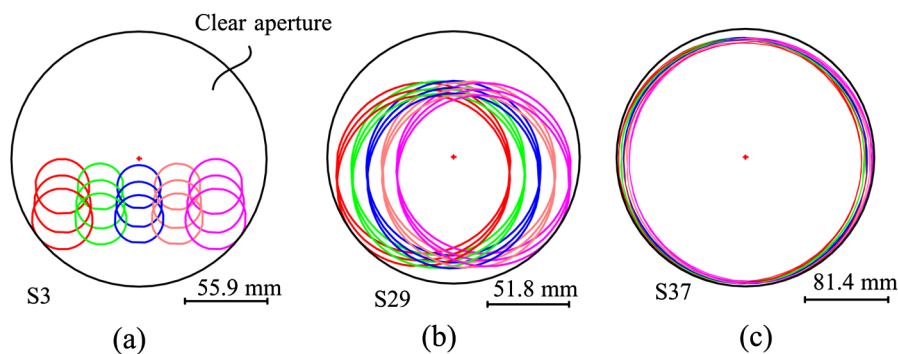


Fig. 3 Footprints of three surfaces of 15 field point of NA 1.2 projection optics (PO): (a) Surface 3, (b) Surface 29, and (c) Surface 37.

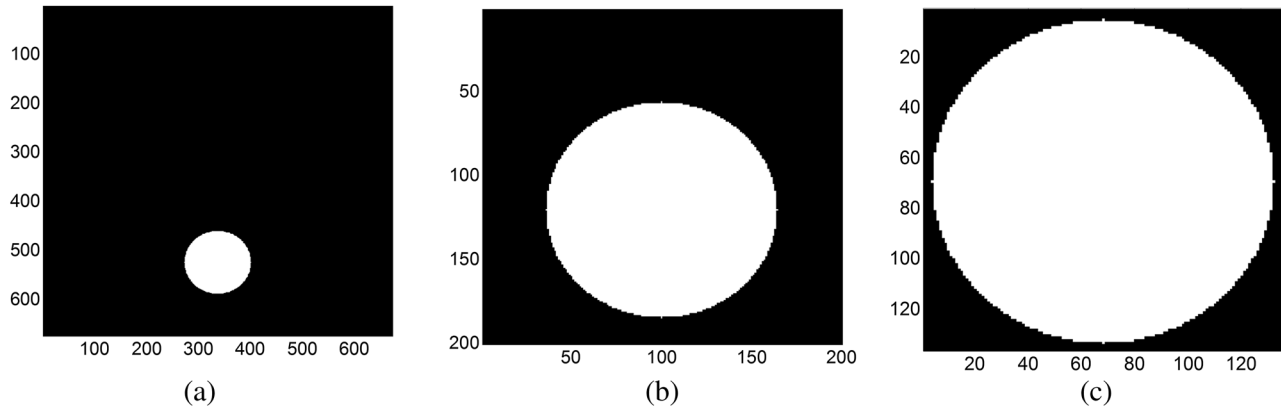


Fig. 4 Masks on three surfaces of F13 (0 mm, 10.1575 mm). (a) on Surface 3, (b) on Surface 29, and (c) on Surface 37.

surfaces for F13 (0 mm, 10.1575 mm), as shown in Fig. 2. The effective intercepted area is shown in white. The matrix elements have a value of one in the white regions, and zero in the black regions.

Finally, the figure-error map S_F on the footprint area for a given rotation azimuth can be obtained from

$$S_F = S_{CA} \cdot M, \quad (7)$$

where S_{CA} is the whole figure-error map in the clear aperture for a given rotation azimuth, and M is the corresponding mask matrix of the given footprint. The operator “ \cdot ” represents the two-dimensional dot product.

The WFE resulting from the figure error W_{system} of each field point for a given clocking angle can be approximated using Eq. (5). The root-mean square (RMS) value of W_{system} is taken as an evaluation indicator to be minimized. In the clocking-optimization program, the RMS of the weighted average of the WFE of multiple field points is expressed as the following function:

$$F(\boldsymbol{\theta}) = \left(\sum_{i=1}^k w_i \times W_{\text{rms}_i} \right) / k, \quad (8)$$

where $\boldsymbol{\theta} = (\theta_1, \theta_2 \dots \theta_j \dots \theta_N)$ is the clocking angle combination of optical components, N is the total number of rotating optical components in the optical system, θ_j is the clocking angle of the j 'th component with respect to the initial orientation, k is the total number of selected field points, w_i is the weighting value of the i 'th field point, and W_{rms_i} is the RMS of W_{system} for the i 'th field point.

The mathematical model for figure-error balancing can be formulated as a combinational optimization problem

$$\min F(\boldsymbol{\theta}) \quad \text{where, } \boldsymbol{\theta} \in \{0, 1, 2 \dots 360\}, \quad (9)$$

where $F(\boldsymbol{\theta})$ is the evaluation function, and $\boldsymbol{\theta}$ is an optimization variable.

The flow chart in Fig. 5 outlines the clocking-optimization method. The initial data include the total number of selected representational field points k , the diameter of the clear aperture for each optical surface, the boundary coordinates of each footprint, the weighting for each field point, the working wavelength, all the surface figure errors, the measuring wavelengths, and so on. Given the footprint boundary

coordinates and the diameter of the clear aperture, the “mask” matrix M of the surface for a given field of view can be obtained. Then the iteration operation of the clocking optimization begins to execute. A new combination of optical-component clocking angles is generated with a random and small perturbation on the basis of the previous angle combination. Considering the resolution of clocking angle, the perturbation range of each clocking angle at each iterative operation is set to be ± 5 deg in the global optimization. The entire figure-error map S_{CA} in the clear aperture on each surface is respectively rotated by the individual new clocking angle. The figure-error maps of these surfaces on the same optical component are rotated by the same clocking angle. Then using corresponding mask matrix of each footprint, the figure-error map on the footprint area

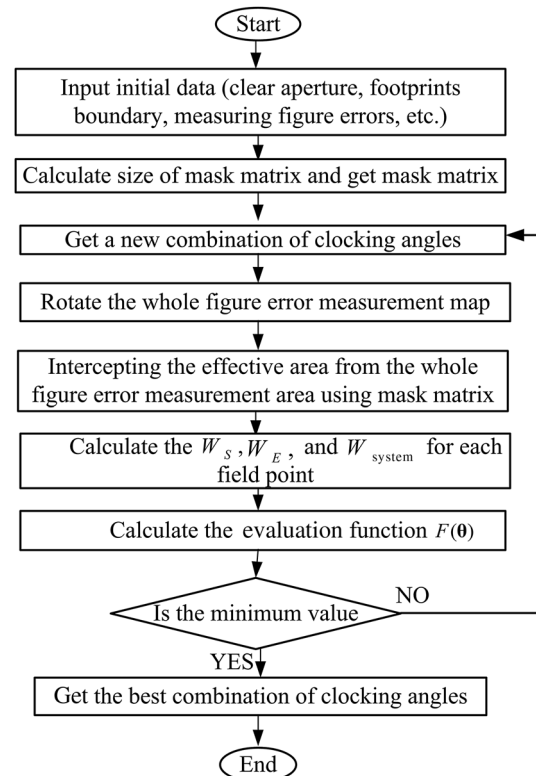


Fig. 5 Flow chart of the clocking-optimization method.

S_F is intercepted from S_{CA} . The interception and rotation of the figure-error map are simplified to the direct operation on the figure-error maps. Therefore, the series complex operations including Zernike fitting, matrix rotation, and discrete point conversion⁷ are not required. For each field point, the WFE caused by the figure error for the given combination of clocking angles is calculated using Eqs. (1)–(5). Then the evaluation function $F(\theta)$ is calculated using Eq. (8). We applied this optimization method to the simulated annealing algorithm to find the globally optimal combination of clocking angles. Finally, the optimal combination of clocking angles for all the optical components was obtained using the global optimization method.

4 Case Study

Two examples, a NA 1.2 lithographic PO and a NA 0.75 small-field PO, were used to demonstrate the effectiveness of the clocking-optimization method.

4.1 Example 1—NA 1.2 Lithographic Projection Optics

The precise lithographic PO is extremely complicated with high manufacturing cost. In order to explore the technique of figure error compensation, a NA 1.2 lithographic PO is designed. The NA 1.2 lithographic PO is shown in Fig. 1. Its optical characteristics are listed in Table 1. It should be noted that we design this optical system only for the purpose of technique development in this paper rather than an applicable lithography lens. The figure-error maps of all optical surfaces are artificial here, but they are useful for validating and verifying the effectiveness of our method.

This PO includes 23 refractive optical components and two concave mirrors, hence 48 optical surfaces in total. Unused regions of the two mirrors were trimmed to avoid beam blocking, and only the effective reflective regions were polished precisely. Therefore, the figure-error maps of the mirrors could not be rotated in the actual assembly process, but their effect on the WFE was considered during clocking optimization nonetheless. The clocking angles of the 23 refractive optical components were taken to be optimizing variables, whereas the two mirrors remained fixed.

Table 1 Optical characteristics of NA 1.2 lithographic projection optics (PO).

| Name | Results |
|---|---|
| Image field size (mm) | 26 × 5 |
| Magnification | 1/4 |
| Wavelength (nm) | 193.368 |
| Image NA | 1.2 |
| Total length (mm) | 1217 |
| Maximum diameter (mm) | 278 |
| Composite wavefront error (WFE) Root-mean square (RMS) (λ) | <0.005 λ ($\lambda = 193.29$ nm) |

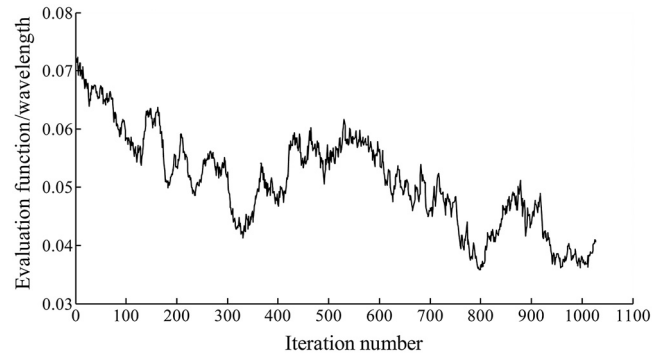


Fig. 6 Evaluation function variation curves for NA 1.2 lithographic PO.

For most surfaces in lithographic projection lens, the peak-valley value (PV) of the surface figure is required less than $1/40\lambda$ ($\lambda = 632.8$ nm). The figure tolerance is so strict that it is almost the most advanced manufacturing level. According to the tolerance requirement, an ensemble of figure-error maps for the 48 surfaces was constructed using Zernike polynomials. The RMS values of the figure errors were between 0.7 and 1.5 nm, and the PVs were between 10 and 25 nm. The figure-error maps were loaded into Code V in the form of an “INT” file for each optical surface. The WFE of the NA 1.2 lithographic PO was deteriorated to 0.097λ (18.8 nm) from the design value of 0.003λ . This shows how high-quality surfaces still produce significant deterioration of the image quality. A compensation method for figure errors is therefore needed to improve image quality.

We applied the automatic figure-error balancing method to this system. Figure 6 shows the variation of the error-evaluation function during the optimization process. As the number of iterations increases, there is an overall decline in the error-evaluation function, with the optimal solution approached after 1027 iterations. The evaluation function decreases to 0.037λ from the initial 0.073λ . The optimal combination of angles of rotation can be acquired automatically after the clocking optimization. The overall running time of the optimization programs is about 12 h.

The method achieves the clocking optimization for mutual figure-error compensation and overcome the shortcoming of currently available commercial optical software. The WFE calculation is simplified by using the footprint data and analytic relation with figure error, and a large amount of real ray traces are not required. The complex distribution of

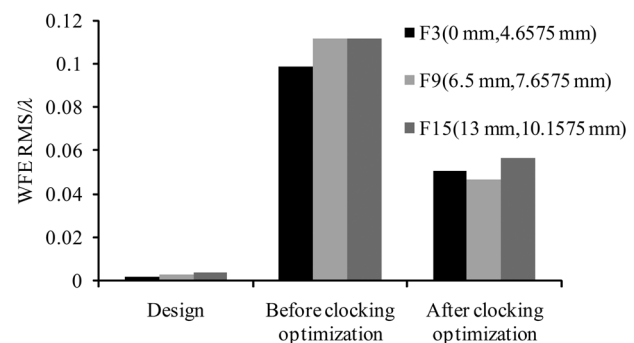


Fig. 7 Contrastive analysis, before and after figure-error balancing, for the NA 1.2 lithographic PO.

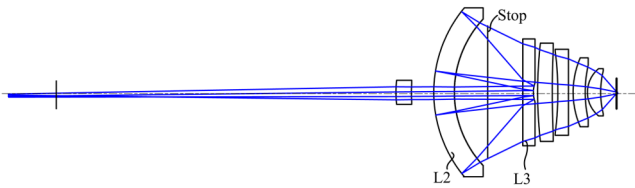


Fig. 8 Two-dimensional layout of the NA 0.75 small-field PO.

real rays on the footprint is assumed as uniform distribution, thus some calculation errors cannot be avoided. Compared with the result calculated by the ray trace method in commercial optical software, the calculation error of WFEs with our method is on the subnanometer level. Despite the existence of the calculation error, an excellent image performance of this system is achieved, when this optimal combination of clocking angles acquired by our method is imported to commercial optical software. In order to make an intuitive impression of the compensation effect, Fig. 7 shows the contrastive analysis, before and after figure-error balancing, for

Table 2 Optical characteristics of the NA 0.75 small-field PO.

| Name | Results |
|--|---|
| Diameter of image field size (μm) | 100 |
| Magnification | -1/40 |
| Spectral band (nm) | 193.29 ± 0.05 |
| Image NA | 0.75 |
| Total length (mm) | 320 |
| Maximum diameter (mm) | 98 |
| Work length in image side (mm) | 9.2 |
| Liner obscuration (%) | 18 |
| Composite WFE RMS (λ) | $<0.030\lambda$ ($\lambda = 193.29 \text{ nm}$) |

three fields of view. The results of the simulation experiment show that the WFE of the NA 1.2 projection lens can be reduced by 43% after figure-error balancing.

The actual WFE may slightly alter the result of the theoretical prediction, because of the testing error of the surface figure and the angle alignment error of the components. However, the clocking-optimization method can indicate the best clocking angle for each component in the initial lens assembly. Thus, the risk of image quality deterioration caused by figure errors of the optical system is largely reduced.

4.2 Example 2—NA 0.75 Small-Field Projection Optics

The NA 0.75 small-field PO is an actual manufacturing optical system used in our lab.¹² This optical system is a catadioptric Schwarzschild lithographic PO system that includes seven optical-components. Its layout of the optical systems is shown in Fig. 8, and its optical characteristics are listed in Table 2.

All surface-figure errors associated with the lens seat were measured with a high-precision Zygo interferometer before

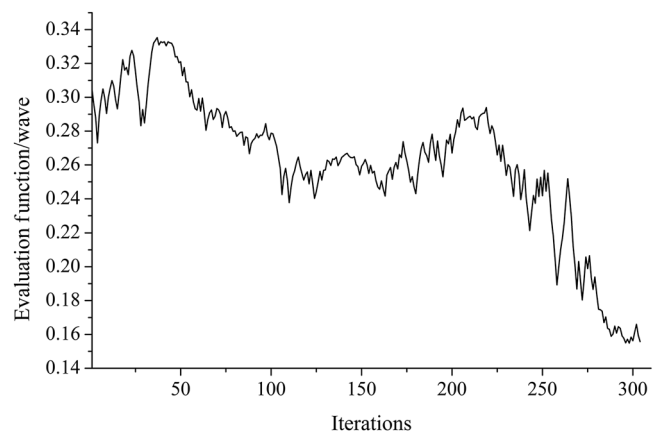
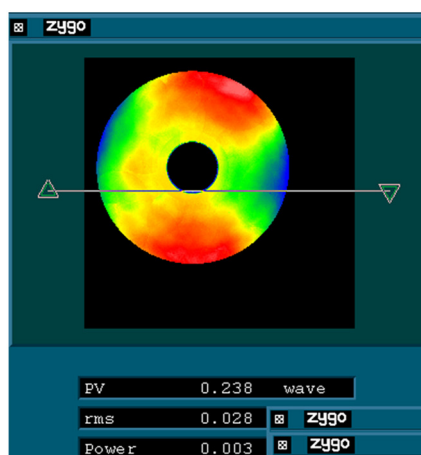
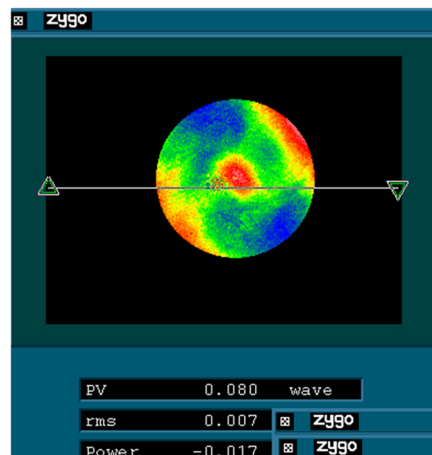


Fig. 10 Error-evaluation function variation for the NA 0.75 small-field PO.



(a)



(b)

Fig. 9 Figure-error maps for the following: (a) the ring-shaped region of the front surface of L2 and (b) the central region of the back surface of L3.

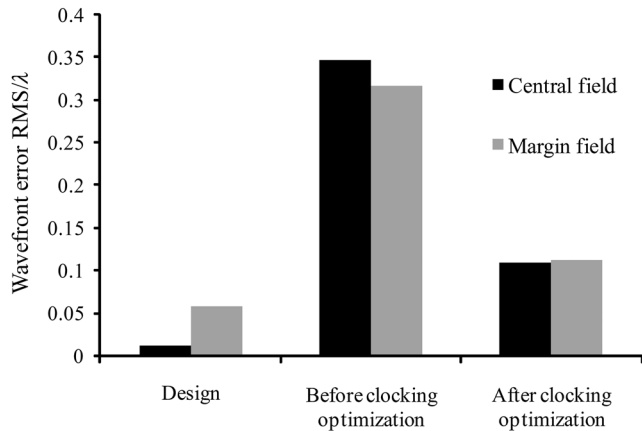


Fig. 11 Contrasting analysis, before and after figure-error balancing, for the small-field PO.

the lens was assembled. Two reflective surfaces were particularly sensitive: the ring-shaped portion of the front surface of L2 and the central portion of the back surface of L3. The figure-error maps for these two reflective surfaces are shown in Fig. 9. Astigmatism is the main contribution to the figure error. For the other surfaces, the figure-error RMS value is around 0.008λ (4.5 nm), and the PV is around 0.05λ . The testing wavelength is 632.8 nm. It is worth mentioning that the coordinate system of the interferometer is different from that defined in Code V for different surface shapes. It is therefore necessary to ensure that the figure-error data are correctly loaded into Code V for each surface.

The clocking-optimization method was applied to this system and Fig. 10 plots the error-evaluation function over 304 iterations. This function reaches a minimal value, from which the optimal angle combination of seven optical components is determined. The overall optimization time was approximately 3 h.

Figure 11 shows a contrasting analysis, before and after figure-error balancing. The WFE for this optical system, after figure-error balancing, was reduced to 0.11λ from 0.35λ ($\lambda = 193.3$ nm). In other words, the final predicting performance of this actual manufacturing system before assembly can be improved to 0.11λ ($\lambda = 193.3$ nm). For this optical system, the simulation results show that about 65% of the WFE is compensated by the automatic figure-error balancing method.

5 Conclusion

This paper proposes a global clocking-optimization method for figure-error balancing in complex optical systems. An accurate and general theoretical model was used to calculate the contributions to the WFE caused by figure errors analytically. The interception and rotation of figure-error maps was achieved using direct operation on the map. The simulated

annealing algorithm was used to determine the optimal combination of clocking angles. This method yields the best mutual compensation among all the figure errors and overcomes the limitations of optical-design software. This method can be applied to coaxial optical-imaging systems with a large field of view, including dioptric, catoptrics, and catadioptric lens systems. However, it is unsuitable for optical systems with vignetting. Nonetheless, this method has considerable engineering potential.

Acknowledgments

This work was supported by the Key Program of the National Natural Science Foundation of China under Grant No. 60938003, the National Science and Technology Major Project, and the Beijing Higher Education Young Elite Teacher Project.

References

1. K. Sugisaki et al., "Influence of fabrication errors on Wolter mirror imaging performance," *Appl. Opt.* **37**(34), 8057–8066 (1998).
2. M. Rimmer, "Analysis of perturbed lens systems," *Appl. Opt.* **9**(3), 533–537 (1970).
3. T. Matsuyama, T. Ishiyama, and Y. Ohmura, "Nikon projection lens update," *Proc. SPIE* **5377**, 730–741 (2006).
4. S. P. Hau-Riege, "Correction of figure errors on optical surfaces by laser-induced contraction of Mo/Si multilayer," *Opt. Lett.* **28**(6), 456–458 (2003).
5. D. M. Williamson, "Compensator selection in the tolerancing of a microlithographic lens," *Proc. SPIE* **1049**, 178–186 (1989).
6. T. Matsuyama et al., "Improving lens performance through the most recent lens manufacturing process," *Proc. SPIE* **5040**, 801–810 (2003).
7. C. Liu et al., "Wavefront aberration compensation of projection lens using clocking lens element," *Appl. Opt.* **52**(22), 5398–5401 (2013).
8. X. Liu, Y. Li, and K. Liu, "Automatic figure errors balancing method for reflective and catadioptric lens," *Opt. Eng.* **53**(3), 035101 (2014).
9. M. J. Riedl, "The Mangin mirror and its primary aberrations," *Appl. Opt.* **13**(7), 1690–1694 (1974).
10. T. Matsuyama et al., "High NA and low residual aberration projection lens for DUV scanner," *Proc. SPIE* **4691**, 687–695 (2002).
11. D. Shafer et al., "Catadioptric projection objective," U.S. Patent No. 20050190435 (2005).
12. X. Liu et al., "Two methods to loosen optical manufacture tolerances for ArF projection optic," *Key Eng. Mater.* **552**, 502–509 (2013).

Xiaolin Liu received her BS degree in optical information science and technology from the Xi'an University of Post and Telecommunication in 2008. Currently, she is a PhD candidate directed by Professor Yanqiu Li in the School of Optoelectronics at the Beijing Institute of Technology. Her current interests include optical system design and fabrication.

Yanqiu Li received her PhD degree in optics from the Harbin Institute of Technology of China. She worked as a senior engineer at Nikon, as an invited professor of Tohoku University of Japan, and as a frontier researcher at RIKEN of Japan. Currently, she is a professor at the Beijing Institute of Technology. She has published numerous articles on lithographic science.

Ke Liu received his MS and PhD degrees in electrical engineering from the Institute of Electrical Engineering, Chinese Academy of Sciences. Currently, he is an associate researcher at the Beijing Institute of Technology, Beijing, China. His research interest is precision optical design and testing.